Simple Modeling Technique for Distortion Analysis of Steel Box Girders

by Geerhard Haaijer*

Abstract

Box-girder bridges are popular around the world because of aesthetics and because of the structural advantages resulting from the high torsional rigidity of box sections. However, thin-wall steel box sections tend to distort when subjected to asymmetric loads across the width of the structure. The distortion of the cross section results in transverse bending stresses and longitudinal normal warping stresses. To reduce these distortional stresses to acceptable levels, internal bracing with diaphragms or cross frames is commonly used in composite steel-concrete box girders.

Analysis of the distortion by classical methods involves considerable mathematical effort that is beyond the scope of most design calculations. Specific bracing requirements could be established with the aid of complex finite-element models in which each component is modeled with appropriate elements such as MSC/NASTRAN QUAD4, BAR and ROD elements. The complete model, however, would have many degrees of freedom and would be costly to run. The present paper demonstrates a simplified approach that requires little computing effort. The concrete deck, webs, and bottom flange of the girder are each represented by a separate string of BAR elements. Through the use of multipoint constraint equations, the displacements of the strings are coupled to satisfy compatibility conditions at the junction of the webs to the concrete deck and bottom flange. Interior bracing members act as supports for the individual BAR strings. The procedure is illustrated by establishing the required spacing of cross frames for a typical mass-transit railway bridge.

* Senior Research Consultant, Research Laboratory, U. S. Steel Corporation, Monroeville, Pa. 15146.

Introduction

Composite box girders consisting of concrete decks and steel webs and bottom flanges are widely used in the construction of bridges for reasons of aesthetics and the structural advantages resulting from the high torsional rigidity of box sections. The structural analysis of box girders is more complicated than that of I girders because the thin-wall steel box sections tend to distort when subjected to asymmetric loads across the width of the structure. The distortion of the cross section results in transverse bending stresses and longitudinal normal warping stresses. To reduce these distortional stresses to acceptable levels, internal bracing with stiffened plate diaphragms or cross frames is commonly used in composite steel-concrete box girders.

The distortion analysis by classical methods[1,2]* involves considerable mathematical effort that is beyond the scope of most design calculations. Specific bracing requirements could be established with the aid of complex finite-element models in which each component is modeled with appropriate elements such as MSC/NASTRAN QUAD4, BAR, and ROD elements. The complete model, however, would have many degrees of freedom and would be costly to run. The present paper describes a simplified approach that makes use of BAR elements only and requires little computing effort.

---

* See References.

General Design Procedure

A typical design situation is shown in Figure 1, illustrating a mass-transit railway bridge subjected to double-track loading. Because maximum longitudinal moments and shears in the girder generally occur when both tracks are loaded, preliminary designs can usually be based on this loading condition. The preliminary design effort can be aided with available computer programs. For example, program SIMON will aid the designer in establishing optimum proportions and dimensions of composite steel box and I girders.[3] This initial design must be checked and possibly modified for the effects of asymmetric loading.

In accordance with the principle of superposition, Figure 2a shows how single-track loading can be split into symmetric loading (Case I) and antisymmetric loading (Case II). Case I loading produces stresses and deflections equal to half those caused by full double-track loading and can be obtained directly from the preliminary design study. Case II loading produces both torsion and distortion in the cross section. These effects can be separated by splitting Case II into two subcases as illustrated in Figure 2b.[2] Case IIa loading produces pure torsion without distortion of the cross section. The forces P/4 and H are applied directly to the webs and flanges, respectively. The magnitude of H is found from the condition that the total applied torsional moment is the same for Cases II and IIa

$$(P/2) * A = (P/4) * A + H * B \quad (1)$$

so that

$$H = (P/4) * A/B \quad (2)$$

In these equations, P is the axle load and H is the horizontal force in the concrete deck and bottom flange A and B are the width and height of the box section.

Because the torsional rigidity of a box section is high, the applied torque is resisted by St. Venant torsion. The resulting shear flow in the cross section can be calculated readily in accordance with established methods for determining torsional stresses in closed sections. Warping normal stresses caused by nonuniform torsion are negligible for a closed section.

The remaining problem involves loading Case IIb, which causes the distortion of the cross section. The analysis of this behavior is discussed next.

Distortion Analysis

The applied forces corresponding to Case IIb are self equilibrating and only distort the cross section. Because the lateral (through-thickness) bending stiffness of the webs and bottom flange is small, the section is assumed to distort as shown in Figure 3. By neglecting the lateral bending stiffness of the steel elements, it is effectively assumed that the connections between the elements behave as piano hinges. The

resulting displacements and warping stresses will be conservative because the actual lateral bending stiffness will somewhat reduce the distortions. Distortional bending stresses are neglected. This simplication makes it possible to use a simple finite-element model. Figure 4 shows how the concrete deck and the steel webs and bottom flange are treated as separate parts. Forces corresponding to axle loads on the complete girder are applied along the length of each part as illustrated in Figure 5 for a two-span continuous box girder. Only the right span is loaded for maximum distortion. Interior bracing is provided at the supports so that the individual parts in Figure 5 are also supported at these locations. Because of antisymmetry only one web needs to be analysed.

The deck, web, and bottom flange are then modeled as strings of BAR elements. The deck, web and bottom flange are artificially placed in the same X-Y plane. Variations in plate width and thickness and the effect of longitudinal stiffeners are easily included in the section properties of the BAR elements. Each grid point has three degrees of freedom: displacement U(1) in the X direction, displacement U(2) in the Y-direction, and rotation U(6) about the Z-axis. From these displacements and rotations, the displacements of the edges of each component can be calculated. Figure 6a shows that the longitudinal displacement of the right edge of the bottom flange is given by

$$DFB = CFB * UB(6) \qquad (3)$$

where UB(6) is the rotation about the Z-axis and CFB is half the width of the flange. Because of antisymmetry, UB(1) (displacement in the X direction) is zero. The displacement UB(2) in the Y-direction does not cause any longitudinal displacement of the edge.

Similarly, Figure 6b shows that the longitudinal displacements of the top and bottom edges of web are given by the following two respective equations

$$DWT = UW(1) - CWT * UW(6) \tag{4}$$

$$DWB = UW(1) + CWB * UW(6) \tag{5}$$

UW(1) is the displacement in the x direction, and CWT and CWB are the distances from the centerline of the web to the midplane of the concrete desk and bottom flange, respectively. Figure 6c shows that the displacement of the top flange at the junction with the web is given by

$$DFT = CFT * UT(6) \tag{6}$$

CFT is half the distance between the two webs. UT(1) is zero from antisymmetry. The constraint equations are obtained from the requirement that displacements of the deck and bottom flange at the junction with the web equal the corresponding displacements of the edges of the web. Thus

$$DFB = DWB \tag{7}$$

and

$$DFT = DWT \tag{8}$$

The resulting equations are

$$CFB * UB(6) - UW(1) - CWB * UW(6) = 0 \tag{9}$$

and

$$CFT * UT(6) - UW(1) + CWT * UW(6) = 0 \tag{10}$$

The coefficients in equations (9) and (10) can be entered directly into the MSC/NASTRAN program through multipoint constraint (MPC) cards.

The output from the program includes the displacements, longitudinal warping stresses caused by the distortion, and reactions at the supports. The latter can be interpreted as loads to be resisted by the internal bracing. Because the above modeling technique assumes that the connection between the components of the box section are hinged, lateral bending is neglected. However, a conservative estimate of the lateral bending stresses could be obtained by making a simple frame model of the cross section and subjecting this model to the displacements determined from the previous analysis. The effect of bracing stiffness could be included with elastic supports.

Design Example

The above procedure will be illustrated by considering the design of a two-span continuous mass-transit railway

bridge. As shown in Figure 7, the spans are 179 and 224 ft, respectively. The structure supports two tracks of loading with axle loads given in Figure 8. These nominal loads are increased by the following impact fraction specified by the American Association of State Highway and Transportation Officials (AASHTO).[4]

$$I = \frac{50}{L + 125} \tag{11}$$

where

I = impact fraction

L = span in ft.

For the span of 224 ft the impact fraction is 0.14. The preliminary design was prepared with the aid of program SIMON on the basis of the AASHTO Load Factor Design (LFD) provisions. ASTM A588 weathering steel was specified for all components. The cross section at the location of maximum positive moment (Section A-A) is shown in Figure 9. Because SIMON was developed for the design of I girders, it considers a box girder as a pair of I girders. Thus SIMON can only consider double-track loading that is symmetrical across the width of the structure. For this condition it develops a design that meets all requirements of AASHTO. Where necessary, SIMON designs appropriate longitudinal and transverse stiffeners. Figure 9 shows one longitudinal stiffener in the compression zone of the web. In the region near the pier where the bottom flange is in compression, the SIMON design included longitudinal flange stiffeners to prevent plate buckling.

At section A-A the maximum live-load stress at the mid plane of the bottom flange is 9.26 ksi caused by full double-track loading. The minimum live-load stress is -1.90 ksi, caused by negative bending at section A-A when the left span is loaded. The total stress range of 11.16 ksi determines the fatigue behavior as checked by SIMON. This stress range is one of the bench marks to establish the need for intermediate diaphragms. The distortion of the section caused by single-track loading should therefore be limited to a range of longitudinal stress less than the above value.

As described in the general procedure, the design developed by SIMON was represented by three strings of BAR elements representing the bottom flange, one of the webs, and the concrete deck, respectively. Table I shows the part of the bulk data that generated the string of bars representing the bottom flange. U. S. Steel's preprocessor PREPPY was used to generate the actual bulk data required by MSC/NASTRAN. Bulk-data cards are generated by inserting cards with the abbreviation DUP in the first field. The numerals following DUP indicate the number of cards to be generated from the preceding card. The values of parameters in the different fields of the DUP cards are used as increments. More complex versions of the DUP cards use sets of preceding cards as the basis for a two-dimensional generation, and generate continuation cards. A total of 24 elements were used for the left span and 30 elements for the right span. Not shown are the PBAR cards describing the properties of the different parts of the bottom flange. Similar bulk-data cards were

prepared for the web and concrete deck. The bulk-data cards representing the constraints are shown in Table II. Grid points 101 through 124 and 201 through 231 define the geometry of the two spans of the bottom flange; grid points 301 through 324 and 401 through 431 are for the web, and 501 through 524 and 601 through 631 are for the concrete deck. The multipoint constraint equations for the NASTRAN model were derived for the left web so that the coefficients have signs different from those shown earlier.

Figure 10 shows the deflected shapes of the concrete deck, web and bottom flange for single-track loading of the right span and internal bracing at the end supports and the pier. Figure 11 illustrates the distortion of the cross section A-A (Figure 7) that results from the deflection of the components. The resulting longitudinal distortion warping stresses in Section A-A are shown in Figure 12. The maximum stress is 9.08 ksi. Because the warping stresses reverse when the other track is loaded, the total stress range will be 18.16 ksi. This significantly exceeds the bench mark of 11.16 ksi for double-track loading . In addition, the indicated distortion would cause significant lateral bending stresses. Because the present analysis is conservative, a more refined analysis could be considered. However, a much improved structure would be obtained by providing internal bracing at additional locations. The effect of additional bracing will be investigated next.

Effect of Intermediate Diaphragms

Some additional internal bracing will be required in any event to facilitate handling during construction. For example, field splices will probably be needed at the junction of the haunched and straight parts of the girder. Cross bracing is customarily provided at field splice locations. Figure 13 shows the effect of bracing at these locations on the deflected shapes of the girder components. The maximum distortion is shown in Figure 14. The corresponding warping stress is reduced to 4.15 ksi (Figure 15). The resulting stress range of 8.30 ksi is within the previously established bench mark.

Finally, the effect of one additional cross frame half way in between the field splice and the end support was investigated. The resulting deflected shapes are shown in Figure 16. The distortions are reduced to almost negligible levels. The horizontal shift of the bottom flange and the vertical deflection of the web are both about 0.04 in. The distortion warping stress is reduced to 1.61 ksi and the stress range is reduced to 3.22 ksi.

Summary and Conclusions

The modeling technique described in the present paper provides a simple method to analyse the effect of internal bracing on the distortion behavior of composite steel-concrete box girders. Table III summarizes the longitudinal stresses at the junctions of the bottom flange and the webs and the horizontal shift of the bottom flange for the different bracing and loading conditions. Placement of two intermediate braces in each

span virtually eliminates distortion of the cross section under single-track loading. In applying the method to a specific structure, attention should be given to the effect of the stiffness of the internal bracing. The present analysis considers the bracing rigid compared with the flexibility of the unbraced sections. The bracing members must be designed to resist the calculated forces. Also, for specific applications, the lateral bending stresses in the webs and flanges should be determined by analyzing the distorted cross section as a rigid frame.

Acknowledgement

The author gratefully acknowledges the contributions of R. L. Mion, U. S. Steel Construction Services, and W. N. Poellet of Richardson, Gordon and Associates in preparing the initial girder design with the aid of program SIMON.

References

1. V. Z. Vlasov, "Thin-Walled Elastic Beams," National Science Foundation, Washington, D.C., 1961.

2. S. R. Abdel-Samad, R. N. Wright, and A. R. Robinson, "BEF Analogy for Analysis of Box Girders," Journal of the Structural Division, ASCE, Vol. 94, No. ST7, July 1968.

3. "SIMON—A Computer Program for the Design of Steel Girders," USS Engineers and Consultants, 600 Grant Street, Pittsburgh, PA.

4. "Standard Specifications for Highway Bridges," Twelfth Edition, American Association of State Highway and Transportation Officials, Washington, D.C., 1977.

Table I

Bulk Data Defining Bottom Flange

```
BEGIN BULK
$MODEL BOTTOM FLANGE
GRDSET                                                          345
GRID     101            0.        0.        0.                1345
DUP16    1              89.5
DUP7     1              89.5                  4.5
GRID     201            2148.     0.        36.               1345
DUP1     1              84.                 -3.324
DUP9     1              90.                 -3.624
DUP19    1              90.
DUP1     1              86.75
CBAR     101    1       101       102       0.        1.      0.
DUP2     1              1         1
CBAR     104    2       104       105       0.        1.      0.
DUP9     1              1         1
CBAR     114    3       114       115       0.        1.      0.
DUP6     1              1         1
CBAR     121    4       121       122       0.        1.      0.
DUP2     1              1         1
CBAR     124    4       124       201       0.        1.      0.
CBAR     201    4       201       202       0.        1.      0.
DUP2     1              1         1
CBAR     204    5       204       205       0.        1.      0.
DUP3     1              1         1
CBAR     208    6       208       209       0.        1.      0.
DUP2     1              1         1
CBAR     211    7       211       212       0.        1.      0.
DUP3     1              1         1
CBAR     215    8       215       216       0.        1.      0.
DUP1     1              1         1
CBAR     217    7       217       218       0.        1.      0.
DUP8     1              1         1
CBAR     226    9       226       227       0.        1.      0.
DUP2     1              1         1
CBAR     229    1       229       230       0.        1.      0.
DUP1     1              1         1
```

Table II

Constraint Data for Coupling BAR Strings

```
$CONSTRAINTS FOR COUPLING ELEMENTS
SPC1      20      1       101     THRU    124
SPC1      20      1       501     THRU    524
SPC1      20      1       201     THRU    231
SPC1      20      1       601     THRU    631
SPC1      20      2       101     201     231
SPC1      20      2       301     401     431
SPC1      20      2       501     601     631
MPC       100     101     6       88.5    301     1       +1.             +M101
+M101             301     6       -42.5
DUP16             1                       1                               +X1
+X1               1
MPC       100     118     6       88.5    318     1       +1.             +M118
+M118             318     6       -44.
DUP6              1                       1                               +Y1
+Y1               1               -2.355
MPC       100     201     6       88.5    401     1       +1.             +M201
+M201             401     6       -60.5
DUP1              1                       1                               +XX1
+XX1              1               +1.72
DUP8              1                       1                               +XY1
+XY1              1               +1.844
MPC       100     211     6       88.5    411     1       +1.             +M211
+M211             411     6       -42.5
DUP20             1                       1                               +XZ1
+XZ1              1
MPC       100     501     6       -88.5   301     1       -1.             +M501
+M501             301     6       -51.
DUP16             1                       1                               +YX1
+YX1              1
MPC       100     518     6       -88.5   318     1       -1.             +M518
+M518             318     6       -52.5
DUP6              1                       1                               +YZ1
+YZ1              1               -2.355
MPC       100     601     6       -88.5   401     1       -1.             +M601
+M601             401     6       -69.
DUP1              1                       1                               +ZX1
+ZX1              1               +1.72
DUP8              1                       1                               +ZY1
+ZY1              1               +1.844
MPC       100     611     6       -88.5   411     1       -1.             +M611
+M611             411     6       -51.
DUP20             1                       1                               +ZZ1
```

Table III

Summary of Results

	SIMON Bending Analysis— Double-Track Loading	NASTRAN Distortion Analysis— Single-Track Loading		
		No Intermediate Brace	One Intermediate Brace	Two Intermediate Braces
Max. Stress,* ksi.	9.26	9.08	4.15	1.61
Min. Stress,* ksi	-1.90	-9.08	-4.15	-1.61
Stress Range,* ksi.	11.16	18.16	8.30	3.22
Horizontal Shift of Bottom Flange, in.	0.0	2.27	0.45	0.04

* Live-load stresses at junctions of bottom flange and webs.

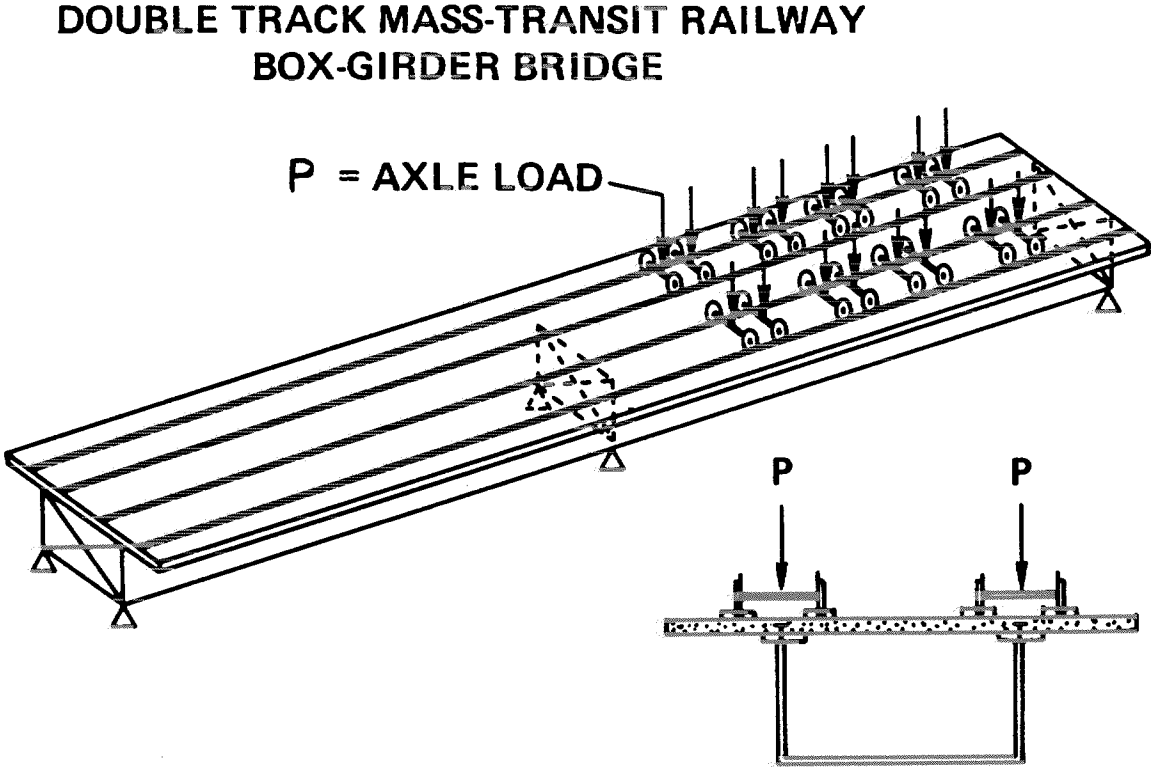

Figure 1 Double Track Mass-Transit Railway Box-Girder Bridge

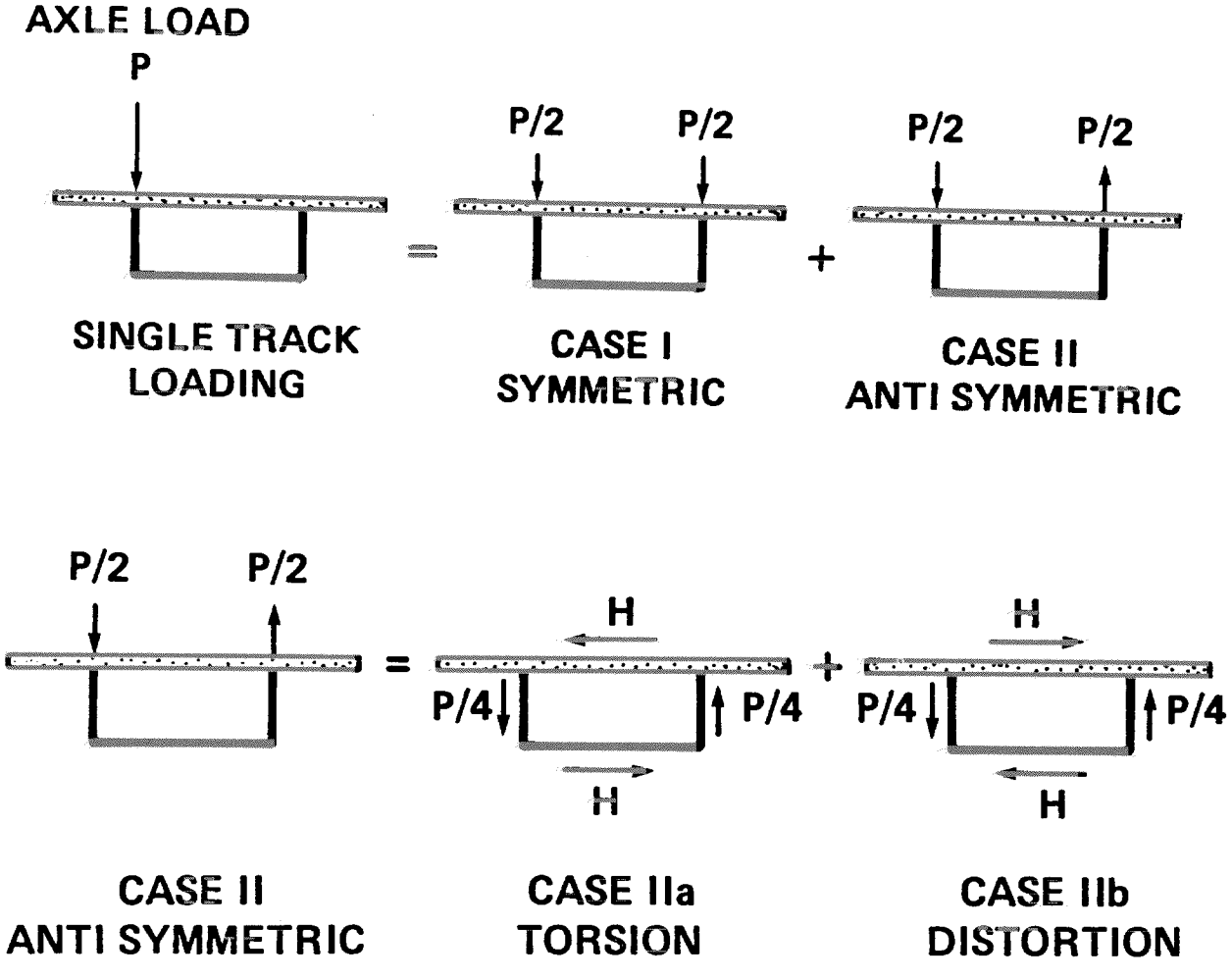

Figure 2 Decomposition of Single-Track Loading

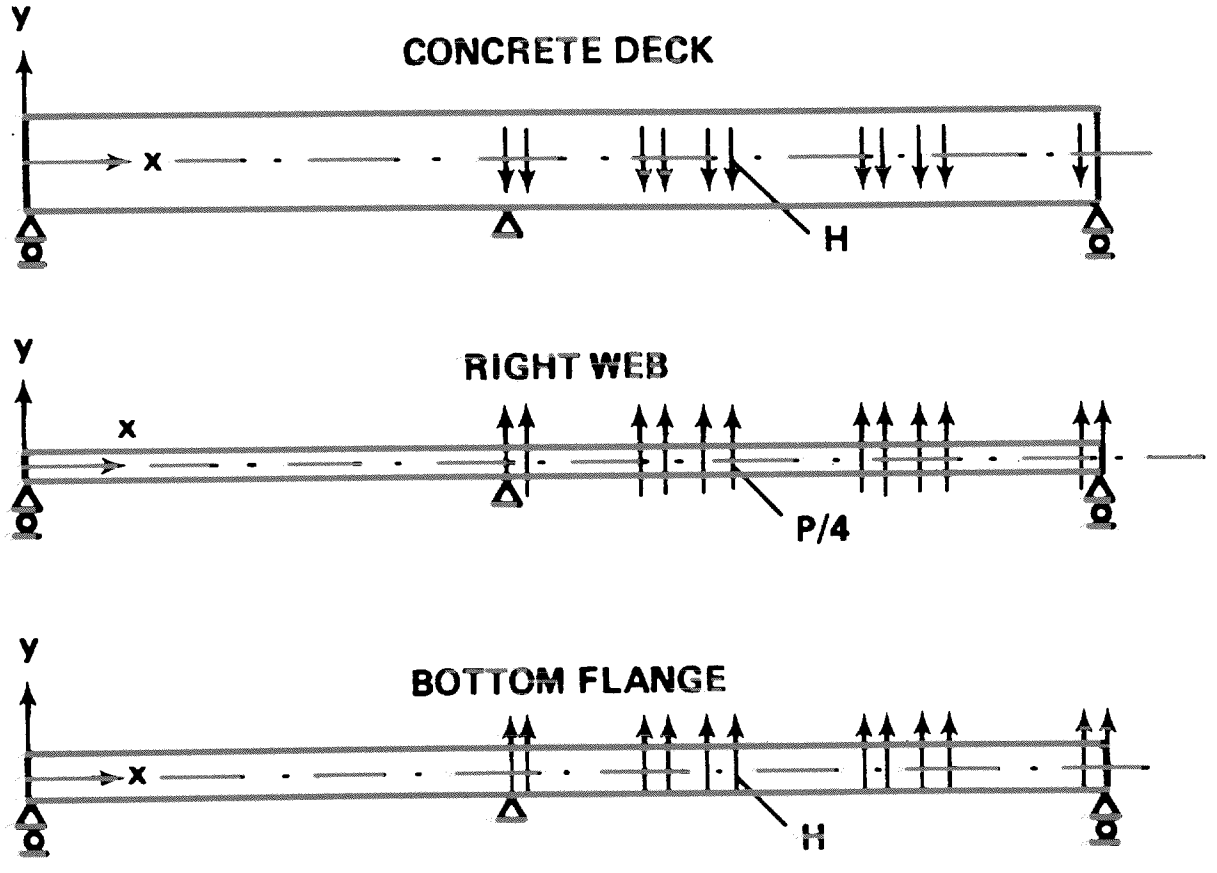

Figure 5 Loading of Cross-Section Components

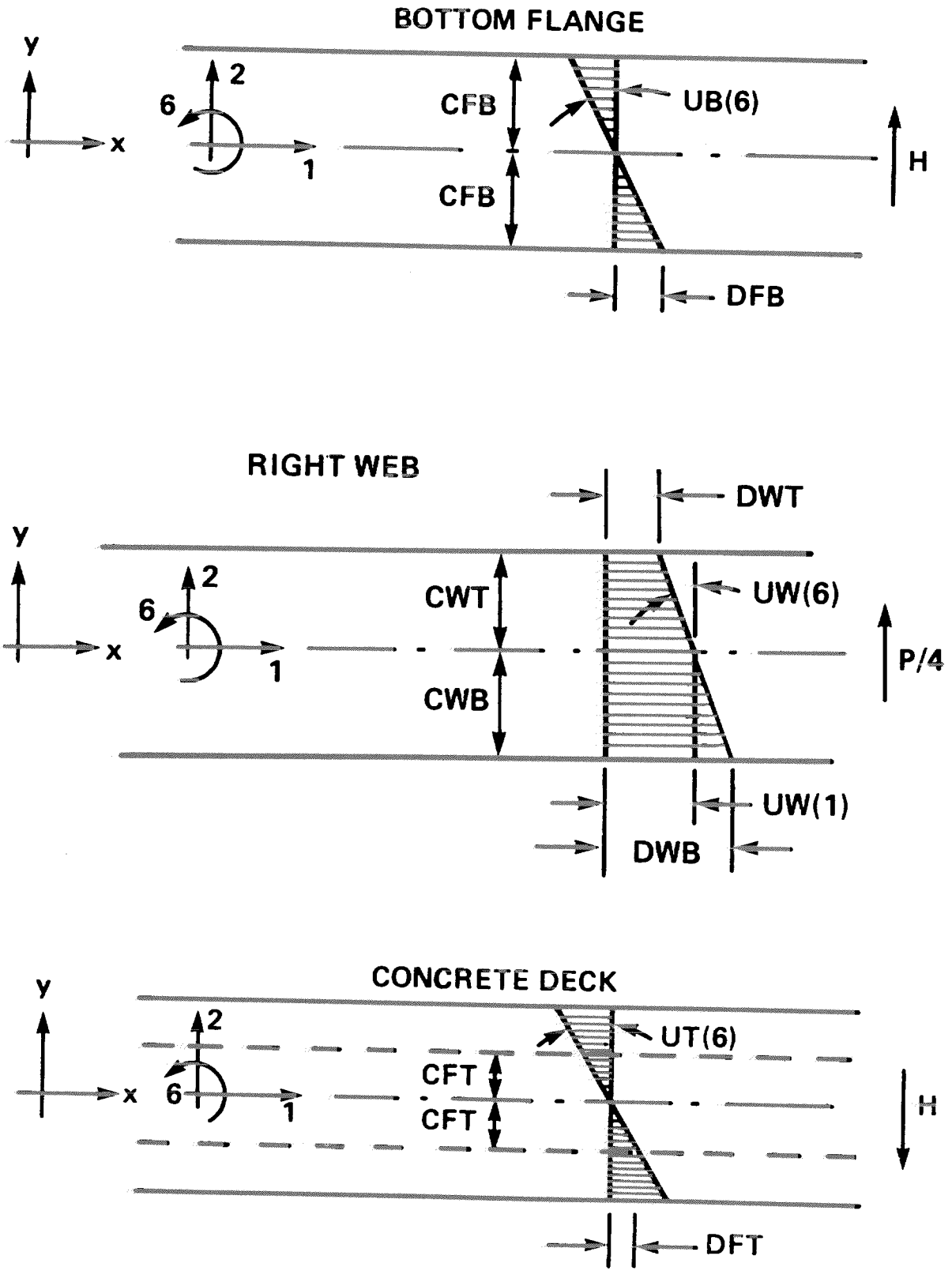

Figure 6 Displacements of Cross-Section Components

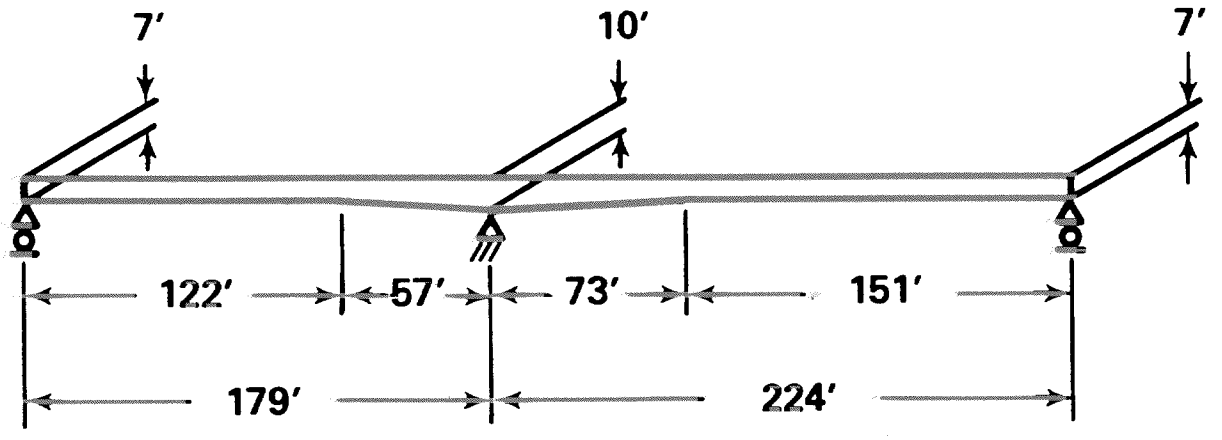

Figure 7 Web Elevation of Mass-Transit Railway Bridge

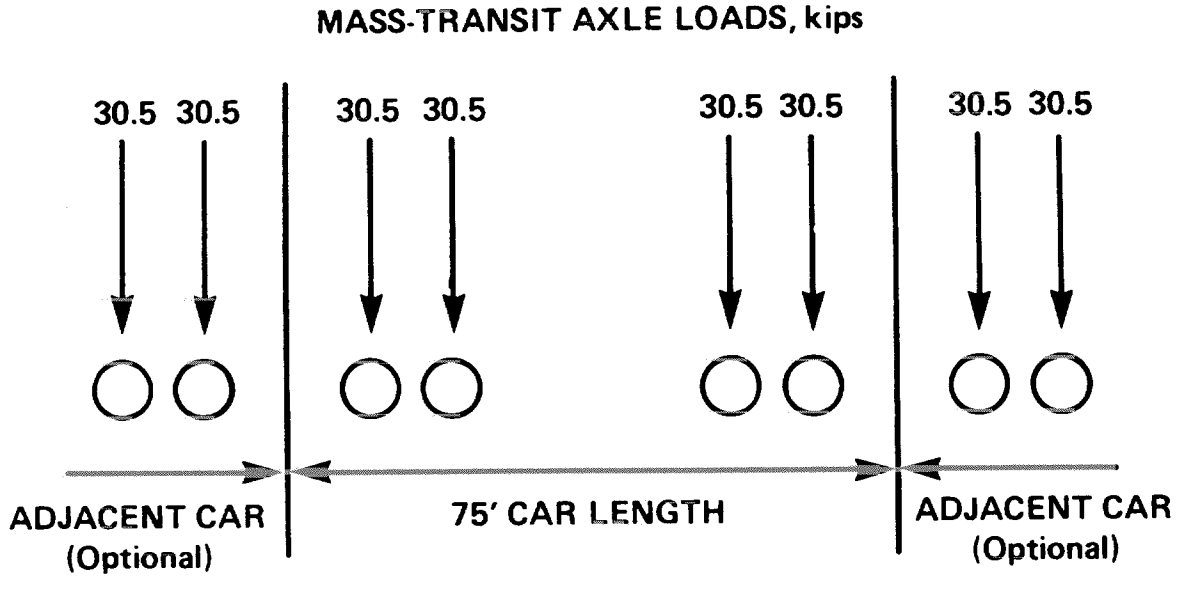

Figure 8 Mass-Transit Axle Loads Used in Present Study

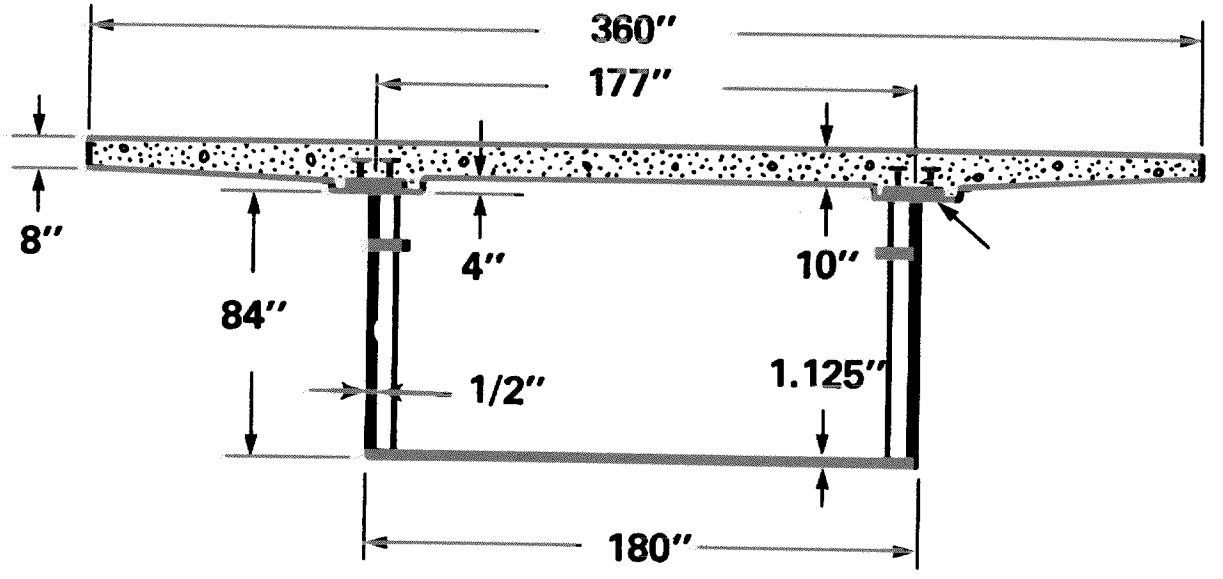

Figure 9 SIMON Design of Positive-Moment Section

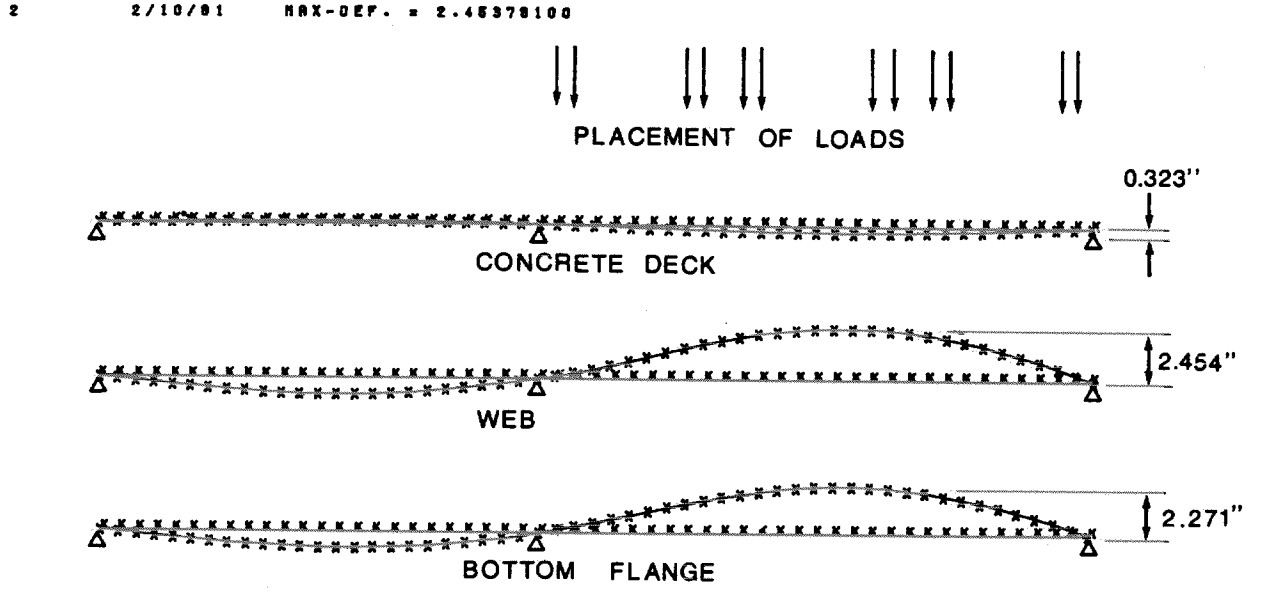

Figure 10 Deformation of Section Components in Absence of Intermediate Bracing

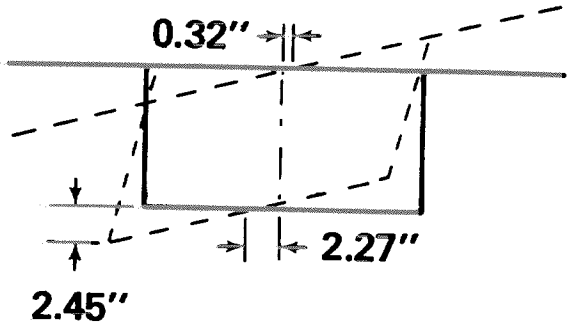

Figure 11 'Maximum Distortion in Absence of Intermediate Bracing

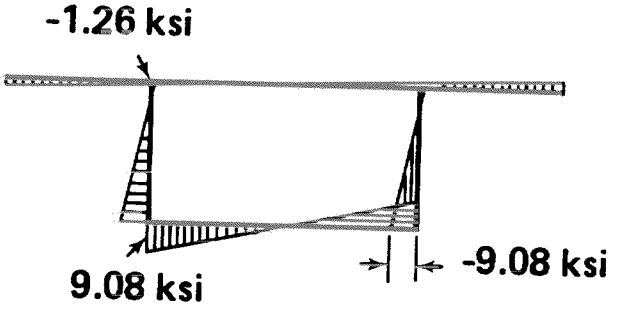

Figure 12 Longitudinal Distortion Warping Stresses in Absence of Intermediate Bracing

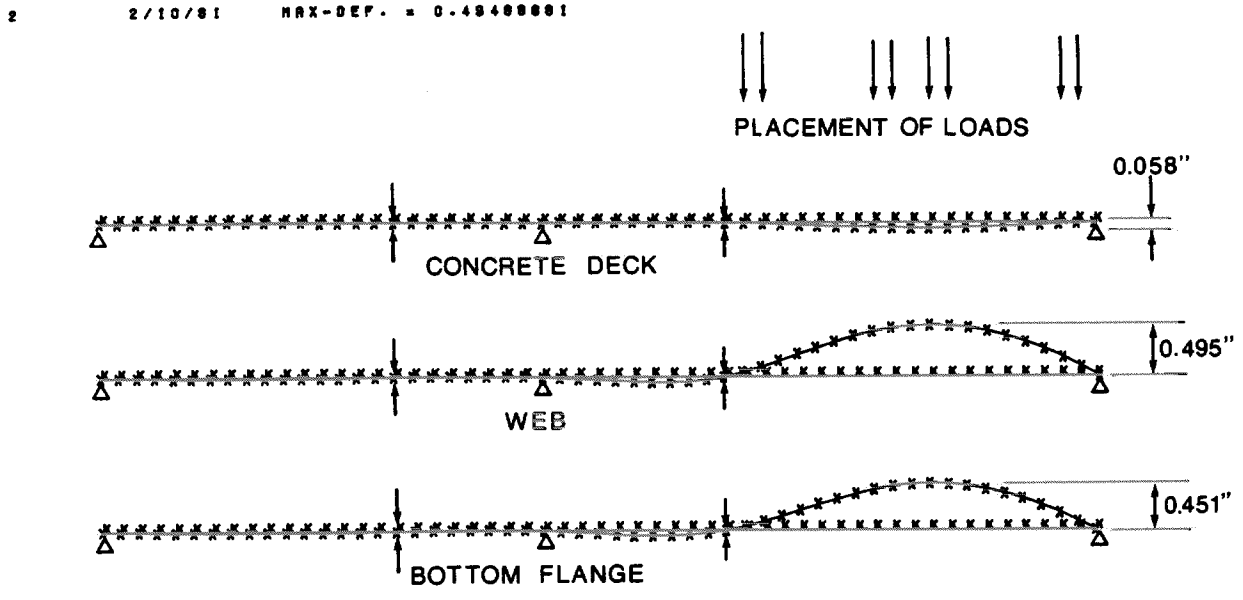

Figure 13 Deformation of Section Components With One Intermediate Brace at Field Splice Location

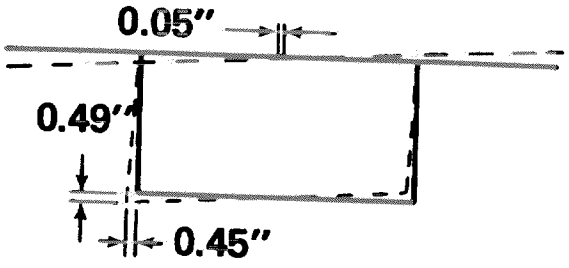

Figure 14 Distortion With One Intermediate Brace at Field Splice Location

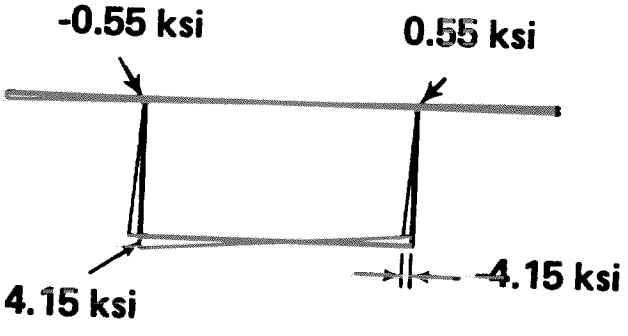

Figure 15 Longitudinal Distortion Warping Stresses With One Intermediate Brace at Field Splice Location

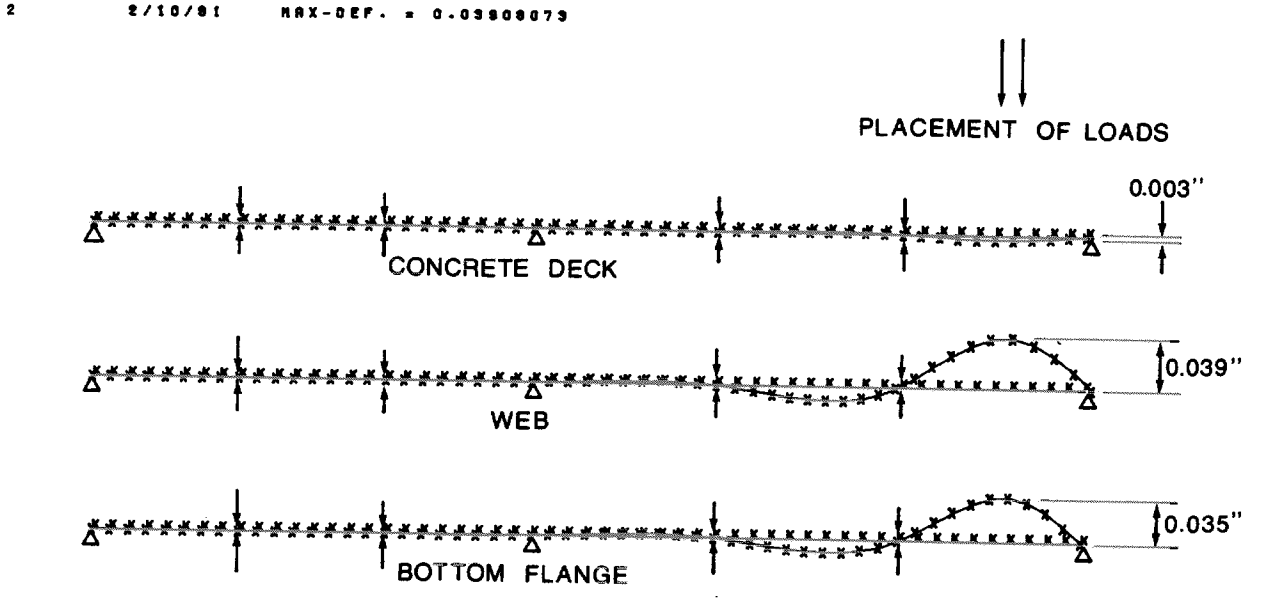

Figure 16 Deformation of Section Components With Two Intermediate Braces in Each Span